Study of Ni sorption onto Tio mine waste rock surfaces

B. Plante [a,*], M. Benzaazoua [a], B. Bussière [a], M.C. Biesinger [b], A.R. Pratt [c]

[a] *Université du Québec en Abitibi-Témiscamingue (UQAT), 445 boul. de l'Université, Rouyn-Noranda, Québec, Canada J9X 5E4*
[b] *Surface Science Western, Room G-1, Western Science Center, University of Western Ontario, London, Ontario, Canada N6A 5B7*
[c] *Natural Resources Canada, CANMET, 555 Booth Street, Ottawa, Ontario, Canada K1A 0G1*

ARTICLE INFO

ABSTRACT

Sorption phenomena are known to play significant roles in metal mobility in mine drainage waters. The present study focuses on sorption phenomena controlling Ni concentrations in contaminated neutral drainage issued from the waste rock piles of the Tio mine, a hematite–ilmenite deposit near Havre-Saint-Pierre, Québec, Canada exploited by Rio Tinto Iron and Titanium. Batch sorption tests were conducted on waste rock samples of different composition and degree of alteration, as well as on the main mineral phases purified from the waste rocks. Sorbed phases were submitted to sequential extractions, XPS and DRIFT studies for further interpretation of sorption phenomena. The results from the present study confirm that sorption phenomena play a significant role in the Tio mine waste rocks, and that the main sorbent phases are the residual ilmenite ore in waste rocks, as well as plagioclase, the main gangue mineral. Sequential extractions suggest that most sorption sites are associated with reducible fractions, and XPS results indicate that Ni is sorbed as the hydroxide $Ni(OH)_2$. The results from the present study provide useful information on sorption phenomena involved in the Tio mine waste rocks and enable further interpretation of Ni geochemistry in contaminated neutral drainage.

1. Introduction

Many toxic metal(loid)s such as Ni, Zn, Co, As and Sb occur in solution at near-neutral pH, and can potentially contaminate mine effluents even without acidic conditions; this phenomenon is called contaminated neutral drainage (CND) or simply Neutral drainage (Pettit et al., 1999; Nicholson, 2004; Bussière, 2007; Heikkinen et al., 2009). For tailings ponds or waste rock piles exposed to atmospheric conditions, these metal(loid)s are often produced by oxidation of sulfide minerals (mainly pyrite and pyrrhotite) which also generates acid in the process. However, when sufficient neutralization is available in the mine wastes and/or when the sulfide oxidation rate is sufficiently slow, CND conditions are maintained (Heikkinen et al., 2009). Many cases can be found in the literature where Ni CND is generated from tailings with significant carbonate neutralization and various sulfide oxidation levels (Heikkinen and Räisänen, 2008; Heikkinen et al., 2009). It has also been demonstrated (Li, 2000) that the silicate contribution to neutralization becomes increasingly important as sulfide oxidation rates drop. Many studies are found in the literature where the unoxidized portion of AMD generating tailings show CND-like features such as near-neutral pH and high dissolved Ni levels (e.g. McGregor et al., 1998; Johnson et al., 2000; Holmström et al., 2001; Gunsinger et al., 2006; Heikkinen and Räisänen, 2008; Heikkinen et al., 2009), where Ni levels are controlled mainly by sorption and/or coprecipitation with Fe oxyhydroxides.

The present study was performed on waste rock sampled from the Tio mine, a hematite–ilmenite deposit near Havre-Saint-Pierre, Québec, Canada. The mine has been in operation since the early 1950s through an open pit operation by Rio Tinto, Fer et Titane Inc. The gangue minerals of the Tio ore are mainly composed of a calcic plagioclase mineral close to labradorite composition, of approximate formulae $Na_{0.4}Ca_{0.6}Al_{1.6}Si_{2.4}O_8$ (Pepin, 2009). The gangue also contains pyroxene, chlorite, mica, biotite and sulfides, mainly pyrite (FeS_2) that is laced with traces of the Ni sulfide, millerite (NiS). Water draining from the waste rock piles are near-neutral and sporadically show Ni concentrations slightly higher than those allowed by applicable local regulations. This is a phenomenon that is referred to as contaminated neutral drainage, or CND (Pettit et al., 1999; Nicholson, 2004; Bussière, 2007).

Other investigations performed on the Tio mine waste rocks have shown that the material is not acid generating in the long term and that Ni is generated mainly from Ni-bearing pyrite and millerite that are associated with ilmenite in the Tio ore. The work also demonstrated that the waste rocks have significant metal retention potential most probably via surface sorption (Bussière et al., 2005; Plante et al., 2008; Pepin et al., 2008; Pepin, 2009; Plante, 2010). Sorption phenomena have been shown to play an important role in metal mobility in tailings (e.g. Gunsinger et al., 2006; Heikkinen and Räisänen, 2008; Álvarez-Valero et al., 2009).

* Corresponding author. Fax: +1 819 797 4727.
  E-mail address: benoit.plante@uqat.ca (B. Plante).

These studies used indirect sequential chemical extractions methods. Studies that make use of direct analysis methods are lacking and are the principal focus of this study.

In the present study, the mineralogy and sorption capacities of waste rocks were investigated in order to better understand the Ni geochemistry in the Tio mine waste rock piles. More specifically, investigations were performed on both waste rock samples and purified fractions of the main minerals found in the Tio mine waste rocks, to determine which minerals are responsible for Ni sorption. Both indirect evaluation of Ni sorption (sequential chemical extractions, sorption tests) and direct measurements (XPS, DRIFT) on the sorbing surfaces are employed to understand the sorption processes involved. The methodology employed in the present study may also be employed to evaluate the extent of sorption phenomena in the control of metal levels in drainage waters.

2. Materials and methods

The Ni sorption behaviour of the Tio mine waste rocks was studied on waste rock samples of different composition and degrees of weathering. In addition, the main minerals in the waste rocks were chosen to be studied separately. Relatively pure mineral fractions were separated from the Tio mine waste rocks. This section details with the sample preparation of waste rock and purified mineral samples, and the methods employed to study Ni sorption mechanisms.

2.1. Waste rock samples (C1–C6) preparation

The mine has been in operation since the early 1950s, and the waste rock piles at the Tio mine are made up of materials that are heterogeneously weathered. Moreover, the material makeup of the waste rock piles varies considerably, as the target cut-off for milling is 76 % hemo-ilmenite (recently changed from 72 %). Also, the mine exploits two different orebodies, namely Tio and North-West, and these have slightly different mineralogical compositions. The waste rock samples were carefully selected to represent the waste rock pile heterogeneity in terms of composition, origin and degree of weathering. All samples were screened to <10 cm at the mine site. Upon arrival at the laboratory, the mine wastes were screened at different size fractions. This study focused on the <500 μm fraction also studied by kinetic testing (Plante, 2010) for the long-term assessment of mine drainage. Even though waste rock dumps contain a wide array of particle sizes ranging from sub-micron to meters, working on the fine fraction is relevant for prediction purposes because the fine-grained fraction of waste rocks comprise the greatest surface area and are, therefore, the most reactive (e.g. Price and Kwong, 1997).

2.2. Purified mineral samples preparation

Relatively pure mineral fractions from the Tio mine waste rocks were prepared at the COREM Laboratory (Québec City, Canada). Many separation methods were combined, such as magnetic and gravimetric separations, and flotation, to obtain relatively pure mineral fractions of the main components of the Tio mine waste rocks: ilmenite, plagioclase, sulfides, mica, chlorite and spinel (Table 1). Some of these fractions (ilmenite, plagioclase and sulfides) were prepared from waste rocks of both ore bodies separately, while the other fractions were combined from both. All fractions were sieved to +200–48 mesh, or 75–300 μm; these purified mineral fractions are referred to as "pure mineral fractions" hereafter, even though a few of these samples contain impurities, as will be shown subsequently.

2.3. Physical, chemical and mineralogical characterization

The specific gravity (G_s) of the waste rock samples was determined with a Micromeritics Helium Pycnometer. The specific surface area (S_s) was determined with a Micromeritics Surface Area Analyser using the BET method (Brunauer et al., 1938) while the grain-size distribution was determined by sieving for the fractions between 10 cm and 0.355 μm and by laser diffraction for the fraction <0.355 μm using a Malvern Instruments Mastersizer S particle size analyzer. The Tio mine waste rock chemical analyses were performed using an acid digestion (HNO_3—Br_2—HF—HCl) followed by ICP-AES analysis of these digests. Silicon is partially evaporated during the digestion procedure and, therefore, was not determined for this study. Sulfide-S was calculated as the difference between acid-extractable SO_4-S and total S measured by ICP-AES. The mineralogical characterization was performed with a Bruker AXS D8 Advance X-ray diffraction (XRD) instrument equipped with Cu radiation. Mineralogical quantification was performed with Rietveld (1993) fitting of the XRD data with the Diffrac^{plus} EVA and TOPAS software from Bruker AXS, allowing a detection limit and precision of up to 0.5 wt.%.

2.4. Blends of purified mineral fractions

An attempt was made to verify the sorption behaviour of simple mineralogical combinations using empirically-derived Ni sorption parameters for individual minerals. The minerals chosen were ilmenite and plagioclase at contents close to those of the waste rock samples, with only one minor mineralogical fraction (chlorite). Plagioclase and ilmenite minerals were chosen in the combinations to reflect the major mineralogy of the wastes, while chlorite was chosen because it showed the highest sorption capacity on a mass basis of the minor minerals studied. The ilmenite (Tio), plagioclase (Tio) and chlorite mineral fractions were mixed in five different combinations, varying from 20% to 60% hemo-ilmenite and from 0.5% to 5% chlorite. These mineral blends are given in Table 2. The specific surface areas, calculated from the weighted average values of the pure mineral fractions given in Table 3, are also included in Table 2 for surface area normalization of the sorption capacities.

2.5. Batch sorption methods (kinetic and static procedures)

The sorption capacities and kinetic parameters were determined using static and kinetic batch sorption tests on pure mineral fractions, simple combinations of three pure minerals (ilmenite,

Table 1
Purification methods for the preparation of the pure mineral samples.

Mineral	Purification methods employed
Ilmenite	Heavy liquid separation, magnetic separation
Plagioclase	Heavy liquid separation, magnetic separation
Sulfides	Flotation
Spinel	Dense liquor, magnetic separation, electrostatic separation
Mica	Flotation, wilfley table, magnetic separation
Chlorite	Dense liquor, magnetic separation, electrostatic separation

Table 2
Pure mineral combinations, in wt.% (S_s: specific surface area).

	Ilmenite	Plagioclase	Chlorite	Total	S_s (m^2 g^{-1})
cl-1	19.62	78.36	2.02	100.00	0.093
cl-2	58.79	39.18	2.03	100.00	0.098
cl-3	59.66	39.80	0.54	100.00	0.090
cl-4	56.98	37.98	5.04	100.00	0.113
cl-5	39.21	58.75	2.04	100.00	0.095

Table 3
Physical characterization of the waste rock and pure mineral samples (G_s: specific gravity; S_s: specific surface area; C_u: uniformity coefficient).

	G_s		S_s (m² g⁻¹)	%<80 μm	D_{10} (μm)	D_{50} (μm)	D_{90} (μm)	C_u
	Meas.	Theor.						
C1	3.09	–	0.837	21	18.3	279.2	603.4	18.6
C2	3.42	–	0.863	32	7.6	194.4	542.2	34.6
C3	3.76	–	0.778	16	34.7	361.0	651.0	12.1
C4	3.27	–	1.932	24	14.7	253.6	585.3	21.6
C5	3.50	–	1.789	23	14.2	270.4	584.5	23.3
C6	3.60	–	1.519	23	14.0	292.9	626.7	25.9
Ilmenite Tio	4.79	4.76–4.86	0.093	2.9	91	164	265	2.09
Ilmenite NW	4.74		0.105	3.0	86	158	262	2.15
Plagioclase Tio	2.69	2.71–2.74	0.080	1.0	99	187	275	2.12
Spinel	3.81	3.95	0.109	10.0	83	160	260	2.18
Mica	2.98	2.8–3.0	0.978	10	81	148	255	1.77
Chlorite	2.83	2.3–3.3	0.591	8.0	83	150	265	2.12

plagioclase and chlorite) and on waste rock samples. A kinetic sorption test was first performed in order to determine the time necessary to reach equilibrium, after which the static tests were performed for the previously determined time. All batch sorption tests were carried out at an initial liquid/solid ratio of 25:1 mL g⁻¹ with the ionic strength adjusted to 0.05 M with NaNO₃. These experimental conditions were chosen after preliminary sorption tests (Plante, 2010) designed after common batch sorption tests found in the literature (e.g. Scheckel and Sparks, 2001a; Nachtegaal and Sparks, 2003; Gu and Evans, 2007; Landry et al., 2009), which enabled sufficient water for sampling during the experiments and significant Ni sorption capacities. The ionic strength adjustments are necessary to limit the effect of a change in ion concentrations on the sorption properties; with a high ionic strength, the composition of the background solution can be considered constant. The initial pH was adjusted using 0.02 M H₂SO₄ and NaOH to 5, 6 and 7; these initial values were selected because they reflect the pH range observed in kinetic studies (Plante, 2010) and in the field (Pepin et al., 2008; Pepin, 2009; Plante, 2010). The sorption kinetics were determined with 10 mg L⁻¹ Ni for all samples except for the mineral blends, whose sorption kinetics were determined at 5 mg L⁻¹. To ensure optimal analytical precision, Ni concentrations utilized to determine kinetic sorption parameters were up to one order of magnitude greater than those observed in the field. The sorption capacities and kinetic parameters were determined in order to appreciate the relative sorption properties of the main minerals present in the waste rock, and to verify to what extent the sorption properties of the waste rocks were predictable from the general mineralogical composition. Prior to batch sorption tests, the pure mineral samples were washed with deionised water and ACS grade ethyl alcohol in order to remove any residual reagents such as collectors, frothers and heavy liquids that had been used during the purification steps (Plante, 2010).

2.6. XPS method

X-ray photoelectron spectroscopy (XPS) was used to gain insight into metal-surface interactions in sorption studies. The batch sorption samples were frozen immediately after the tests for conservation and thawed just prior to XPS analyses. The samples were placed on an adhesive and transferred wet into the introduction chamber of the XPS. The water was then pumped away in the introduction chamber. This method effectively limits air exposure of the samples. Analyses were carried out using a Kratos Axis Ultra X-ray photoelectron spectrometer using a monochromatic Al Kα source (15 mA, 14 kV). The XPS method, which can detect all elements except for H and He, probes the surface of the sample to a depth of 7–10 nm, and has detection limits ranging from 0.1 to 0.5 atomic% depending on the element. Survey scan analyses were

carried out with an analysis area of 300 × 700 μm and pass energy of 160 eV. The survey scans were used for surface quantification measurements. Also, high resolution analyses were carried out for certain elements with an analysis area of 300 × 700 μm and pass energy of 20 eV. High resolution analyses allow for an examination of the chemical states present in each area studied. The Kratos charge neutralization system was used during all analyses. All spectra were charge corrected to the main line of the C 1s spectrum (adventitious C) set to 284.8 eV. Additional details concerning the XPS method and instrumentation can be found in Grosvenor et al. (2006), Pratt et al. (2007) and Biesinger et al. (2009) and references therein.

2.7. DRIFT spectra collection

Diffuse Reflectance Infrared Fourier Transform (DRIFT) spectroscopy was employed to study the surface functional groups modified by metal sorption. DRIFT spectra were collected on sorbed ilmenite and plagioclase purified fractions to verify if sorption processes induce a change in the surface vibrational properties of these minerals. The DRIFT spectra were collected on a Bruker Optics Tensor 27 Fourier Transform Infrared Spectrometer. The spectra were acquired with 128 scans at a resolution of 2 cm⁻¹ from 400 to 4000 cm⁻¹, with the aperture set to 4 mm. The samples were ground and sieved to <45 μm and the spectra were obtained on samples diluted to 15 wt.% with spectrograde KBr powder purchased from Harrick Scientific Products.

2.8. Sequential extractions

Sequential extractions are utilized to selectively dissolve groups of geochemically similar mineral phases. Results from sequential extractions provide insight on metal removal mechanisms (e.g. Neculita et al., 2008). Sequential extractions are widely used to evaluate metal mobilization in soils (e.g. Zagury et al., 2009) and mine wastes (e.g. Gunsinger et al., 2006; Heikkinen and Räisänen, 2008; Álvarez-Valero et al., 2009). However, sequential extractions are considered as semi-quantitative methods to evaluate the nature and quantity of metal-removal sites in soils and mine wastes. Replicate sequential extractions on sorbed waste rock samples showed less than 10% standard deviation with a mean value of 6% (Plante, 2010).

The sequential extraction method that was utilized in this study was adapted from the work of Neculita et al. (2008) and is summarized in Table 8: (1) the soluble and easily exchangeable phases were extracted using 0.5 M MgCl₂ at pH 7 for 1 h at room temperature, (2) the acid-soluble phases were extracted with 1 M sodium acetate at pH 5 for 5 h at room temperature and (3) the reducible phases were extracted with NH₂OH–HCl 0.04 M in 25 % acetic acid

for 6 h at room temperature. The extractions were performed on 1–2 g aliquots under ambient air and on a rotary shaker at 250 RPM to minimize any diffusion-related bias. The effectiveness of the sequential extraction procedure in retrieving the sorbed Ni was tested with samples C1 and C4, by performing sequential extractions on aliquants previously submitted to batch sorption tests at 10 mg L^{-1} Ni and pH 6, using the same conditions as in batch sorption tests described in Section 2.4. The results on fresh and weathered waste rock samples showed sorbed Ni recovery between 93% for fresh waste rocks and 106% for weathered waste rocks. The fact that more than 100% of Ni is recovered in weathered waste rock samples may be due to Ni sorbed in the field prior to sampling. However, mass balance errors among the various extracted fractions may also explain the recovery levels obtained. Sequential extractions inherently result in carryover of dissolved ions with moisture remaining from previous extractions. Furthermore, individual extractions will extract phases intended to be extracted in subsequent steps. These issues, combined with analytical errors, will result in mass discrepancies when using sequential chemical extractions. In order to minimize possible carryover between extraction steps, the samples were rinsed twice with deionized water after a chemical extraction step; these water extracts were combined with the corresponding chemical extraction for metal analysis.

3. Theoretical background

3.1. Sorption kinetics

Sorption phenomena are influenced by experimental conditions such as pH, temperature, the nature of the metal ion to be sorbed and its initial concentration, the nature of the sorbing surface, the liquid to solid ratio and the ionic strength of the solution (e.g. Limousin et al., 2007). The sorption kinetics were analyzed using pseudo-second order, Elovich, intra-particle diffusion and liquid film diffusion models (e.g. Sen Gupta and Bhattacharyya, 2006, 2008; Subramanyam and Das, 2009). The pseudo-second-order kinetics model is expressed as follows:

$$\frac{1}{q_t} = \frac{1}{K_2 q_e^2} + \frac{t}{q_e} \tag{1}$$

where q_t is the sorbed quantity (mg g^{-1}) at time t (min), q_e is the sorbed quantity at equilibrium (mg g^{-1}) and K_2 is the second-order reaction rate (g mg^{-1} min^{-1}). The Elovich model is used to express second-order kinetics, assuming that the sorption occurs on energetically heterogeneous surfaces:

$$q_t = \beta \ln(\alpha\beta) + \beta \ln t \tag{2}$$

where α and β are the Elovich coefficients and represent the initial sorption rate (mg g^{-1} min^{-1}) and the desorption constant (g mg^{-1}), respectively. The intra-particle diffusion model, which best describes the sorption processes where diffusion of the ion to be sorbed through the inside of the particle plays a significant role in the kinetics, is defined as:

$$q_t = K_p t^{\frac{1}{2}} \tag{3}$$

where K_p is the intra-particle diffusion rate constant (mg g^{-1} s$^{-1/2}$). However, when diffusion of the ion to be sorbed through the liquid phase surrounding the particle plays a significant role in the sorption kinetics, the liquid film diffusion model best describes the sorption kinetics; it is defined as:

$$\ln\left(1 - \frac{q_t}{q_e}\right) = -K_{fd} t \tag{4}$$

where K_{fd} is the liquid film diffusion rate constant (min^{-1}).

3.2. Sorption isotherms

Nickel sorption by the pure minerals and waste rock samples was studied using the Langmuir, Freundlich and Temkin sorption isotherms. The Langmuir isotherm assumes monolayer coverage of sorption of each molecule onto the surface has equal activation energy of sorption (Chen et al., 2008). The Langmuir isotherm is expressed as follows:

$$q_e = \frac{q_m C_e}{1/b + C_e} \tag{5}$$

Or, in its linear form:

$$\frac{C_e}{q_e} = \frac{1}{b q_m} + \frac{C_e}{q_m} \tag{6}$$

where q_e is the sorbed Ni by sorbent mass at equilibrium (mg g^{-1}), C_e is the equilibrium Ni concentration (mg L^{-1}), q_m is the maximum sorbed Ni by sorbent mass (mg g^{-1}) and b is the sorption equilibrium constant (L mg^{-1}).

The Freundlich isotherm model is considered to be appropriate for describing both multilayer sorption and sorption on heterogeneous surfaces (Ho et al., 2002; Coles and Yong, 2006). It is expressed as follows:

$$q_e = K_c C_e^{\frac{1}{n}} \tag{7}$$

where q_e is the sorbed Ni (mg g^{-1}), K_c is the Freundlich constant, C_e is the equilibrium Ni concentration (mg L^{-1}) and n is the affinity constant; this equation is often used in its logarithmic form for the linear relationship:

$$\log q_e = \log K_c + \frac{1}{n} \log C_e \tag{8}$$

The Freundlich isotherm is linear as long as $1/n = 1$ (for $n = 1$); when $1/n$ decreases, the isotherm becomes less linear. Since the K_c values are dependent upon the $1/n$ values, K_c values are only comparable when $1/c$ values are similar. Therefore, K_c values cannot be considered as an analog to the distribution coefficient between the liquid and solid phases (Chen et al., 1999; Coles and Yong, 2006).

The Temkin isotherm considers the interactions between the sorption surface and the metallic ions to be sorbed and is based on the hypothesis that the sorption energy is a function of surface coverage (Chen et al., 2008):

$$q_e = \frac{RT}{b_T} \ln(A_T C_e) \tag{9}$$

where A_T is the equilibrium binding constant corresponding to the maximum binding energy, b_T is the Temkin isotherm constant, T is the temperature (K), and R is the ideal gas constant (8.315 J mol^{-1} K^{-1}).

The Dubinin-Radushkevich isotherm is valid at low concentration ranges and can be used to describe mono layer coverage over homogeneous or heterogeneous sorption sites (Tan et al., 2008). It is expressed in its linear form as follows:

$$\ln q_e = \ln X_m - BF^2 \tag{10}$$

where q_e is the sorbed Ni at equilibrium expressed in mol L^{-1}, X_m is the maximum uptake capacity (mol g^{-1}), B a constant related to energy (mol^2 kJ^{-2}) and F the Polanyi potential, which is calculated with the following:

$$F = RT \ln\left(\frac{1}{1 + \frac{1}{C_e}}\right) \tag{11}$$

where R is the gas constant (J mol^{-1} K^{-1}), T the absolute temperature (K) and C_e the Ni concentration at equilibrium (mol L^{-1}). The

mean free sorption energy E (kJ mol^{-1}) is calculated using the previously determined B parameter following (Wang et al., 2007; Tan et al., 2008; Hasan et al., 2009):

$$E = \frac{1}{\sqrt{2B}} \tag{12}$$

The E value can be used to estimate the type of sorption for the particular sorbent–surface couple studied. It is generally assumed that if the sorption energy is below 8 kJ mol^{-1}, the sorption can be affected by physical forces such as Van der Walls forces (Özcan et al., 2006), while if E is between 8 and 16 kJ mol^{-1}, the sorption is governed mainly by ion exchange (Wang et al., 2007; Tan et al., 2008; Hasan et al., 2009). Sorption may be governed by particle diffusion if $E > 16$ kJ mol^{-1} (Tan et al., 2008).

4. Results and discussion

4.1. Physical properties

The physical characteristics of the waste rock and pure mineral samples are given in Table 3. The G_s of the waste rocks varies from 3.087 to 3.764 and follows the ilmenite content of the samples. The G_s of the purified mineral samples is close to the theoretical values (see Table 3) of the pure minerals, indicating that the separations were successful. The mean G_s of the ilmenite fractions was calculated using the mean weighted value from 75 wt.% ilmenite ($G_s = 4.72$) and 25 wt.% hematite ($G_s = 4.9$–5.3), which is the ratio suggested by XRD data (Table 6). The S_s of the waste rock samples is lower for the fresh (0.778–0863 m^2 g^{-1}) than for the weathered waste rock samples (1.519–1.932 m^2 g^{-1}), probably because of the greater surface roughness generated by weathering. Some characteristics of the grain-size distribution (% < 80 μm, D_{10}, D_{50}, D_{90} and the uniformity coefficient, $C_u = D_{60}/D_{10}$) are also given in Table 3, showing that the weathered waste rock samples are generally finer than the fresh ones. Since the pure fractions were sieved to 75–300 μm, the % > 80 μm are low (1.0–10%), and the D_{10} (81–99 μm), D_{50} (148–187 μm) and D_{90} (255–275 μm) values are generally in accordance with the sieving.

4.2. Chemical and mineralogical characterization

The chemical and mineralogical characterization of the waste rock and pure mineral samples are shown in Table 4. In the waste rock samples, the Fe (12.8–30.7 wt.%) and Ti (5.99–14.70 wt.%) contents followed the hemo-ilmenite contents targeted for the study. The S contents from sulfide minerals were higher in the fresh waste rock samples (0.543–0.755 wt.%) than in the weathered ones (0.215–0.382 wt.%) and followed the ilmenite contents. The Ni, Co, Cu, Cr and Sb contents tended to follow the ilmenite and sulfide concentrations in the waste rock samples. The elements related to silicate minerals (Ca and Al) followed an inverse trend to that of ilmenite. The pure mineral sample chemical compositions clearly showed that the Ni, Co, Cu and Zn were mostly associated with the sulfides, while Cr, Mn and Sb were associated mainly with hemo-ilmenite. In addition to their association with sulfides, Ni and Co were also associated with ilmenite. Calcium was mostly associated with plagioclase but also with chlorite, while Al was associated mainly with plagioclase, and to chlorite and mica to a lesser degree. Magnesium was associated almost equally with mica and chlorite.

The purified ilmenite fractions (Tio and NW ores) did not contain XRD-detectable minerals other than ilmenite (73.3–73.6 wt.%) and hematite (25.5–26.7 wt.%). The plagioclase fraction was composed of 98.5 wt.% labradorite and 1.5 wt.% chlorite. The sulfide fractions (Tio and NW) were composed of 85 wt.% pyrite,

3.8–7.1 wt.% chalcopyrite and up to 2.4 wt.% millerite. The non sulfide minerals that completed the sulfide fractions were gehlenite, hedenbergite, muscovite, chlorite and quartz. The mica sample did not contain XRD-detectable minerals other than muscovite. The spinel sample was composed of 81 wt.% hercynite, with 9 wt.% labradorite, 5 wt.% quartz and minor amounts of hemo-ilmenite. The chlorite fraction contained only 35 wt.% chlorite, with 49 wt.% labradorite and 11 wt.% muscovite, with minor amounts of calcite and hemo-ilmenite.

In the waste rock samples, the hemo-ilmenite contents obtained ranged between 30 and 40 wt.%, which is different from what was targeted (20–60 wt.%) during sampling, due to plagioclase enrichment in finer fractions of the samples (Pepin, 2009). The labradorite and hemo-ilmenite content represented roughly 80 wt.% of the mineralogy of the waste rock samples. Chlorite (3–8 wt.%), augite (a pyroxene mineral, 2–7 wt.%) akermanite (1–8 wt.%) and hercynite (a spinel mineral, 0.2–3.5 wt.%) complete most of the mineral composition, with pyrite, pyrrhotite, chalcopyrite, muscovite, chlorite and quartz in minor amounts. The augite and akermanite minerals were used in the XRD interpretation of the waste rock samples instead of hedenbergite and gehlenite because they fit the data better. Further studies would be needed to identify more precisely the mineral found in the samples within the gehlenite–akermanite and augite–hedenbergite solid solution series. However, these identifications are not necessary for the goals of the present study.

4.3. Sorption kinetics

The sorption kinetics obtained are displayed in Fig. 1 for the pure minerals (a), waste rock samples (b) and pure mineral combinations (c). The rapid Ni uptake in the first minutes of the experiments may be due to the large amount of sorption sites available at the beginning; as the sorption sites are gradually filled up, sorption becomes slower (Jeon et al., 2003; Bhattacharyya and Sen Gupta, 2008). The rapid initial sorption may also be due to slow conversion from outer-sphere to inner-sphere complexes due to increasing surface charge (Jeon et al., 2003). The Ni sorption follows pseudo-second-order kinetics; the second-order kinetics parameters obtained by best fit (k_2 in min g mg^{-1} and min m^2 g^{-1}, as well as determination coefficients R^2 obtained from linear regressions) are given in Table 5. The second order constant k_2 were normalized with regard to sample weight (min g mg^{-1}) and specific surface areas (min m^2 mg^{-1}) to account for differences in grain-size distribution between the waste rock and pure minerals samples. The R^2 values for pseudo-second order are all greater than 0.99 except for the ilmenite Tio (0.986), and spinel (0.973) samples. The ilmenite NW ore sample is best described by the Elovich, intra-particle diffusion or the liquid film diffusion models for the period over which the sorption kinetics are studied.

The sorption kinetics of the mineral combinations (Fig. 1c) were very close to one and other, even though their compositions differed. They are also similar to those of the pure ilmenite and plagioclase samples. Thus, it seems that the presence of minor amounts of other minerals do not affect the overall sorption behaviour of the waste rocks in simple mineral combinations, even when those minerals show much faster sorption kinetics.

The sorption kinetics enabled the estimation of the time necessary for equilibrium in batch sorption tests. The batch sorption tests were used to evaluate the sorption capacities in different conditions of pH and for Ni concentrations. Since the weathered waste rock samples never reached equilibrium within the 4320 min (72 h) equilibration time, the batch tests for the weathered waste rock samples compared the Ni capacities obtained after 4320 min of equilibration. These results are given in the next sections.

Table 4
Chemical and mineralogical characterization of the waste rock samples (in wt.%).

Elements		C1	C2	C3	C4	C5	C6	Ilmenite Tio	Ilmenite NW	Plagio. Tio	Sulfides Tio	Sulfides NW	Mica	Spinel	Chlorite
Al		9.26	6.86	4.65	6.46	5.30	4.74	0.341	0.431	13.0	0.267	0.208	7.85	2.08	8.66
Ca		4.50	3.27	2.30	3.09	2.37	2.11	0.060	0.090	6.56	0.179	0.211	0.777	0.151	2.75
Co		0.020	0.031	0.042	0.024	0.033	0.034	0.049	0.044	0.000	1.11	0.880	0.012	0.009	0.007
Cr		0.020	0.032	0.054	0.046	0.055	0.063	0.085	0.057	0.001	0.002	0.000	0.035	0.043	0.014
Cu		0.023	0.041	0.046	0.025	0.032	0.032	0.006	0.013	0.002	1.39	2.26	0.020	0.007	0.013
Fe		12.8	20.6	30.7	17.5	26.3	29.3	42.3	43.0	0.431	51.4	52.1	9.89	5.70	13.5
Mg		0.954	1.51	1.71	3.06	2.58	2.56	1.56	1.65	0.196	0.172	0.177	9.60	2.50	7.73
Mn		0.035	0.054	0.074	0.073	0.075	0.079	0.107	0.103	0.002	0.002	0.000	0.015	0.031	0.023
Ni		0.022	0.049	0.044	0.031	0.032	0.038	0.031	0.028	0.002	1.75	2.28	0.036	0.018	0.072
S		0.543	0.533	0.755	0.215	0.350	0.382	0.186	0.287	0.032	44.7	45.4	0.143	0.084	0.125
Sb		0.007	0.013	0.019	0.010	0.014	0.024	0.064	0.058	0.001	0.001	0.000	0.003	0.001	0.005
Ti		5.99	10.8	14.7	7.70	11.1	12.2	20.1	18.8	0.057	0.303	0.066	3.93	1.50	0.943
Zn		0.004	0.005	0.005	0.007	0.006	0.006	0.005	0.005	0.004	0.142	0.043	0.016	0.055	0.013
Mineral	Formulae														
Labradorite	$(Ca,Na)(Si,Al)_4O_8$	ND	52.1	37.1	51.4	43.0	42.0			98.5				9.4	48.7
Ilmenite	$FeTiO_3$	ND	22.9	27.7	20.0	26.6	27.9	73.3	73.6					1.9	1.0
Hematite	Fe_2O_3	ND	7.4	8.2	8.1	9.7	10.0	26.7	25.5					2.4	1.2
Pyrite	FeS_2	ND	1.8	2.3	1.0	1.5	1.8				85.1	85.4			
Pyrrhotite	FeS	ND	1.0	1.5	0.9	1.1	1.1				0.2				
Chalcopyrite	$CuFeS_2$	ND	0.1	0.1	0.1	0.1	0.2				3.8	7.1			
Millerite	NiS											2.4			
Gehlenite	$Ca_2Al(AlSi)O_7$	ND	0.8	1.6	1.0	0.4	0.5				2.8	2.3			
Augite	$Ca_2MgSi_2O_7$	ND	2.4	2.9	6.8	3.6	3.2								
Hedenbergite	$CaFeSi_2O_6$										1.5	1.3			
Muscovite	$KAl_2(Si_3Al)O_{10}(OH,F)_2$	ND	1.7	1.8	1.0	1.5	2.0					0.3	100.0		11.3
Chlorite	$(Mg,Fe,Al)_6(Si,Al)_4O_{10}(OH)_8$	ND	6.0	3.0	5.3	8.1	6.7			1.5	4.7				34.6
Calcite	$CaCO_3$	ND	1.0	1.4	0.3	0.6	0.3								3.2
Quartz	SiO_2	ND	1.8	1.1	2.3	2.2	1.7				1.8	1.2		5.2	
Akermanite	$(Ca,Na)(Mg,Fe,Al,Ti)(Si,Al)_2O_6$	ND	0.8	7.7	1.4	1.5	1.6								
Hercynite	$FeAl_2O_4$	ND	0.2	3.5	0.6	0.3	0.8							81.2	
	Total	ND	100.0	99.9	100.2	100.2	99.8	100.0	99.1	100.0	99.9	100.0	100.0	100.1	100.0
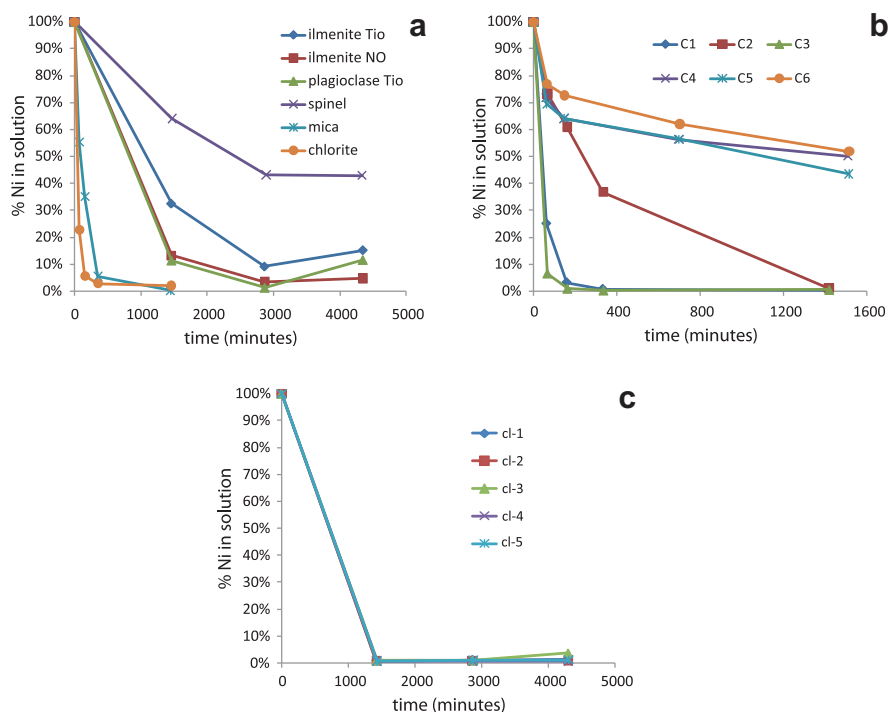
Fig. 1. Ni sorption kinetics in 0.05 M $NaNO_3$, pH 6 and 10 mg L^{-1} Ni on pure minerals (a) and waste rock (b) samples and 5 mg L^{-1} for mineral combinations (c).

Table 5
Kinetic model verification for Ni sorption at 10 mg L^{-1} and pH 6 at 72 h.

	Pseudo-second order				Elovich	Intra-particle diffusion		Liquid film diffusion	
	R^2	q_e (mg g^{-1})	k_2 (min m^2 mg^{-1})	k_2 (min g mg^{-1})	R^2	R^2	k_i (mg min$^{-0.5}$ g^{-1})	R^2	k_{fd} (s^{-1})
C1	0.999	0.243	0.483	0.028	0.850	0.802	3.42E−03	0.657	4.30E−04
C2	0.995	0.227	0.044	5.22E−03	0.994	0.979	2.95E−03	0.908	1.93E−04
C3	1.000	0.249	1.96	0.145	0.872	0.630	3.24E−03	0.585	6.32E−04
C4	0.999	0.122	0.456	0.065	0.972	0.734	1.61E−03	0.696	3.96E−04
C5	0.995	0.141	0.272	0.028	0.967	0.791	1.84E−03	0.758	3.00E−04
C6	0.998	0.112	0.226	0.050	0.978	0.737	1.45E−03	0.709	3.38E−04
Ilmenite Tio	0.986	0.205	1.07E−03	0.012	0.727	0.927	2.99E−03	0.767	1.97E−04
Ilmenite NW	0.999	0.221	3.23E−03	0.031	0.796	0.884	3.43E−03	0.777	6.18E−04
Plagioclase Tio	0.995	0.206	0.380	4.753	0.198	0.859	3.33E−03	0.629	3.74E−04
Spinel	0.973	0.156	6.24E−04	5.73E−03	0.866	0.968	1.95E−03	0.874	2.38E−04
Mica	0.999	0.197	0.094	0.096	0.826	0.694	4.53E−03	0.536	7.54E−04
Chlorite	1.000	0.217	0.310	0.524	0.580	0.471	4.47E−03	0.341	1.18E−03
cl-1	1.000	0.124	−0.107	−1.15	0.999	0.838	2.00E−03	ND	
cl-2	1.000	0.128	−0.237	−2.42	1.000	0.839	2.07E−03		
cl-3	1.000	0.124	−0.019	−0.210	0.599	0.832	2.01E−03		
cl-4	1.000	0.124	−1.55	−13.8	0.869	0.840	1.99E−03		
cl-5	1.000	0.128	−0.133	−1.40	0.929	0.839	2.06E−03		

4.4. Ni sorption on waste rock and pure minerals samples

The sorption capacities at equilibrium (q_e) for 10 mg L^{-1} Ni at pH 5, 6 and 7 of the fresh (C1–C3) and weathered (C4–C6) waste rocks and pure minerals are shown in Fig. 2a–d. The sorption capacities are normalized per mass (mg kg^{-1}, Fig. 2a and b) and per surface area (mg m^{-2}, Fig. 2c and d); the sorption capacities normalized to surface area were obtained by dividing the sorption capacities per mass (mg kg^{-1}) by the specific surface area of the sample (m^2 kg^{-1}). These results show that Ni sorption is greater at pH 6 for all waste rocks and pure mineral samples; the differences are greater for the waste rock samples than for the pure mineral samples. The sorption capacities of the fresh waste rocks shown in Fig. 2a and c (q_e around 1000 mg kg^{-1} or 1.15–1.35 mg m^{-2}) are greater than those of the weathered ones (q_e

of 400–500 mg kg^{-1} or 0.25–0.55 mg m^{-2}) for 10 mg L^{-1} Ni at pH 6, either on a mass or surface basis. On a mass basis, the sorption capacities (at 10 mg L^{-1} Ni and pH 6) shown in Fig. 2b and d for the ilmenite and plagioclase samples (300–450 mg kg^{-1}) are greater than that of spinel (240 mg kg^{-1}) but lower than mica (590 mg kg^{-1}) and chlorite (620 mg kg^{-1}). However, the ilmenite and plagioclase sorption capacities on a surface basis (3.3–5.7 mg m^{-2}) are higher than all other minerals considered (0.5–2.1 mg m^{-2}). Since the sorption capacities of all samples were better at pH 6, the influence of Ni concentrations on sorption behaviour was studied at pH 6; the sorption capacities for pH 6 at 1, 10 and 25 mg L^{-1} Ni are shown in Fig. 2e–h. The results confirm that the fresh waste rocks possess greater sorption capacities than the weathered waste rocks, both on the basis of mass and surface area. The results on pure mineral fractions show that
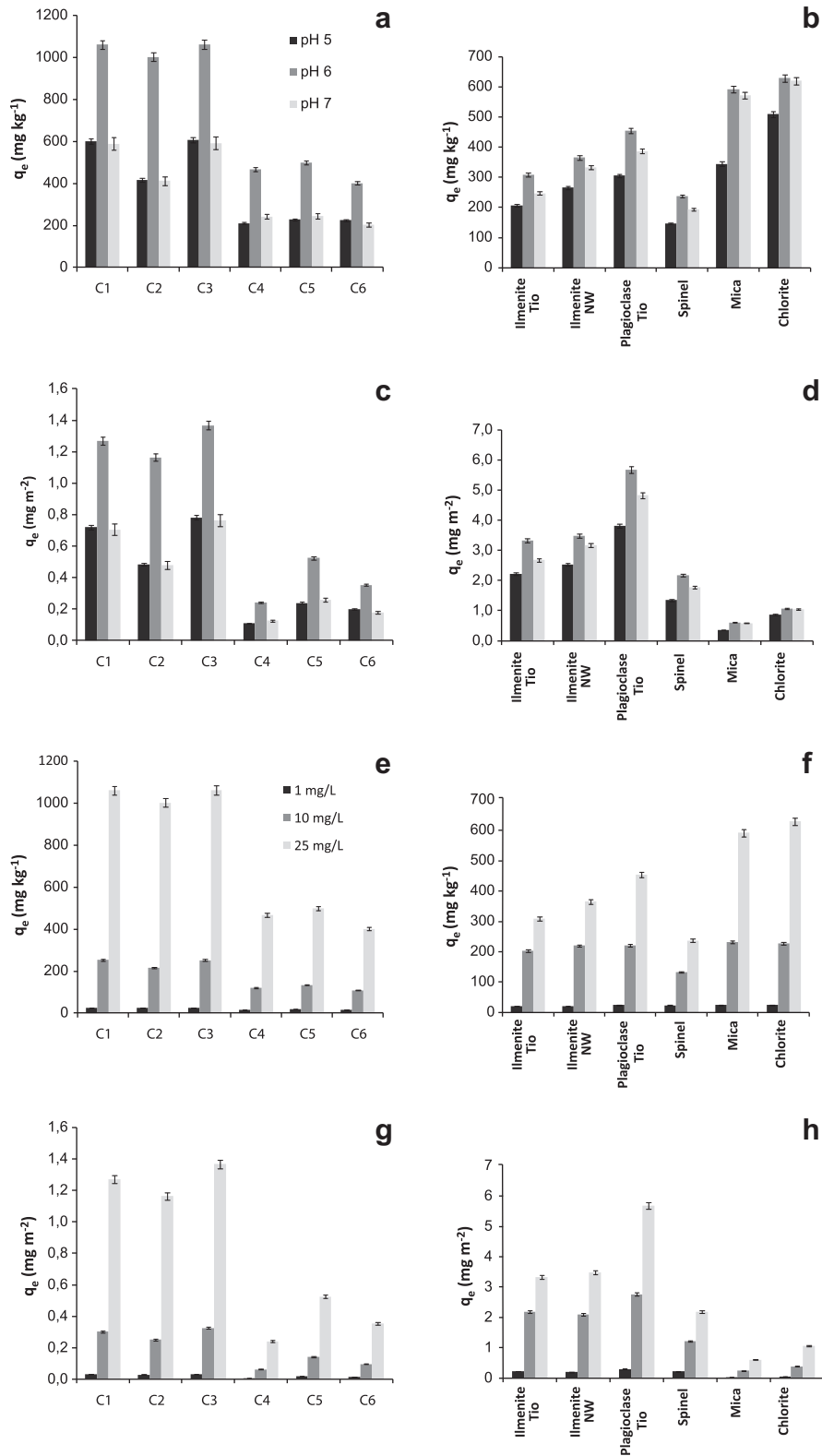
Fig. 2. Ni sorption capacities (q_e): at pH 5, 6 and 7 for 25 mg L^{-1} Ni of the waste rock (per mass, a and per surface area, c) and pure mineral samples (per mass, b and per surface area, d), and at pH 6 for 1, 10 and 25 mg L^{-1} for the waste rock (e and g) and pure mineral samples (f and h).

plagioclase is the most effective Ni sorbent (on a surface basis) in the Tio mine waste rocks, with sorption capacities up to twice those of ilmenite, the second most effective Ni sorbent in the pure minerals studied.

4.5. Sorption isotherms

The sorption capacities may be analyzed in terms of different sorption isotherms, which suggest additional interpretations

Table 6
Sorption isotherms at 25 mg L^{-1} Ni as a function of pH (5, 6 and 7) and at pH 6 as a function of Ni concentration (1, 10, 25 mg L^{-1}).

	Langmuir			Freundlich			Temkin			Dubinin-Radushkevick		
	R^2	q_m (mg g^{-1})	b (L mg^{-1})	R^2	K_c	$1/n$	R^2	A_T (L mg^{-1})	b_T	R^2	B (mol^2 kj^{-2})	E (kJ mol^{-2})
pH dependance of sorption isotherms												
C1	1.000	0.465	−16.7	0.993	0.267	−0.615	0.992	1.11	−4996	0.994	−3.9E−03	ND
C2	1.000	0.365	−1.10	0.999	1.22	−0.533	0.999	0.041	−6972	0.999	−4.4E−03	ND
C3	0.995	0.469	−35.9	0.973	0.164	−0.625	0.977	2.44	−4884	0.975	−3.8E−03	ND
C4	0.852	0.060	−0.090	0.694	11,625	−3.98	0.645	0.055	−1959	0.697	−0.039	ND
C5	0.993	0.059	−0.090	0.999	26,265	−4.29	1.000	0.056	−1718	0.999	−0.042	ND
C6	0.915	0.022	−0.072	0.932	9.8E+13	−12.3	0.952	0.061	−673	0.932	−0.121	ND
Ilmenite Tio	1.000	0.111	−0.120	0.993	6.96	−1.22	0.981	0.029	−8029	0.994	−0.012	ND
Ilmenite NW	1.000	0.169	−0.174	0.999	2.42	−0.802	0.995	0.022	−9975	0.999	−7.8E−03	ND
Plagioclase Tio	0.996	0.223	−0.259	0.998	1.53	−0.609	1.000	0.019	−10,883	0.997	−5.7E−03	ND
Spinel	1.000	0.063	−0.085	0.995	41.6	−1.87	0.980	0.032	−7113	0.995	−0.019	ND
Mica	0.999	0.321	−1.11	0.985	0.700	−0.276	0.988	4.98E−03	−19,716	0.980	−2.4E−03	ND
Chlorite	1.000	0.507	−25.3	0.996	0.569	−0.060	0.995	5.26E−08	−72,645	0.996	−4.5E−04	ND
Concentration dependance of sorption isotherms												
C1	0.621	−2.21	−3.14	0.999	14.1	3.13	0.835	193	8227	1.000	6.2E−03	9.0
C2	0.367	0.413	4.30	0.829	0.369	1.90	0.424	81.1	19,331	0.829	4.1E−03	11.1
C3	0.987	−0.423	−14.3	0.987	63.2	4.18	0.716	207	7046	0.982	7.6E−03	8.1
C4	0.003	11.8	0.003	0.977	0.035	2.51	0.709	2.13	22,866	0.964	7.2E−03	8.3
C5	0.130	0.108	0.402	0.977	0.049	2.30	0.716	2.96	23,006	0.964	6.4E−03	8.8
C6	0.098	0.081	0.346	0.976	0.033	2.34	0.721	2.21	27,495	0.964	6.7E−03	8.6
Ilmenite Tio	0.991	0.339	0.785	0.779	0.103	1.73	0.932	16.9	41,025	0.826	4.3E−03	10.8
Ilmenite NW	0.946	0.426	0.574	0.560	0.131	1.67	0.806	23.1	35,949	0.588	4.0E−03	11.1
Plagioclase Tio	1.000	0.460	10.7	0.903	0.281	1.46	1.000	488	44,793	0.948	2.4E−03	14.4
Spinel	0.955	0.254	0.613	0.997	0.091	1.38	0.900	129	91,060	0.989	2.2E−03	15.1
Mica	0.968	0.669	4.72	0.612	0.515	1.64	0.922	184	23,562	0.626	3.2E−03	12.5
Chlorite	0.276	0.689	5.29	0.924	1.38	2.21	0.603	193	20,934	0.922	4.56E−03	10.5

regarding the sorption modes on the surfaces. The pH dependence of the sorption isotherms was verified at 25 mg L^{-1} for pH 5, 6 and 7 and modeled with the Langmuir, Freundlich Temkin and Dubinin-Radushkevich (DR) isotherms; the isotherm characteristics are shown in Table 6. These isotherms may all be adequately used to describe the systems studied here; their applicability for the samples studied will be verified in the following. All waste rock samples, except for C4 and C6, were fit reasonably well with the 4 considered isotherms (R^2 values of 0.973–1.000 for all waste rock samples except for C4, with R^2 values of 0.645–0.852 and for C6, with R^2 values of 0.915–0.952). All pure mineral samples were fit reasonably well with the four considered isotherms, with R^2 values in the range of 0.980–1.000. Therefore, it is difficult to establish from these isotherms whether Ni sorption occurs as a monolayer or as a multilayer process, at homogeneous or heterogeneous sorption sites, or if sorption is a function of surface coverage.

The concentration dependence of sorption isotherms was verified at pH 6 with Ni concentrations of 1, 10 and 25 mg L^{-1} and modeled with the Langmuir, Freundlich and Temkin isotherms; the isotherm characteristics are shown in Table 6. The pure mineral sorption results are best described by the Langmuir isotherm (R^2 values from 0.946 to 1.000, but for chlorite, the R^2 is of 0.276),

which assumes equal activation energy of sorption, as mentioned beforehand; thus, the Langmuir isotherm seems appropriate to model relatively pure phases which offer fairly homogeneous sorption sites. Since the chlorite sample contains three different major minerals (over 10 wt.%), it is likely that an isotherm considering the surfaces to be homogeneous (such as the Lamgmuir isotherm) will not fit the data in a satisfactory manner. The only pure mineral sample results that are fit reasonably well by the Temkin isotherm is the plagioclase sample (R^2 = 1.000 while other minerals all have R^2 < 0.932). The Temkin isotherm considers the interactions between the sorption surface and the metallic ions to be sorbed and is based on the hypothesis that the sorption energy is a function of surface coverage (Chen et al., 2008).

The waste rock sample sorption results are best described by the Freundlich isotherm (R^2 values from 0.977 to 0.999 but for C2, R^2 = 0.829), which is considered to be appropriate for describing both multilayer sorption and sorption on heterogeneous surfaces (Ho et al., 2002; Coles and Yong, 2006). Since sorption on the pure mineral samples is best explained by the Langmuir isotherm which considers monolayer sorption, the fact that the Freundlich isotherm best fits the waste rock sorption results suggests heterogeneous sorption surfaces rather than multilayer
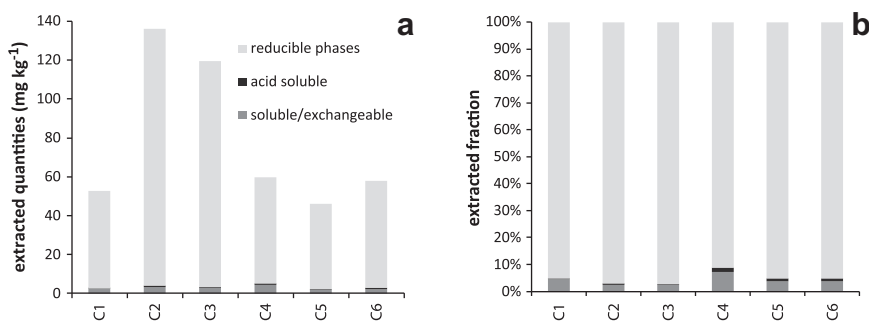
Fig. 3. Absolute (a) and normalized (b) sequential extractions results for Ni in the waste rock samples.

surface coverage. The DR isotherm fits the sorption data reasonably well for the waste rock samples (R^2 of 0.964–1.000 except for C2, with 0.829), but not for the pure mineral samples (R^2 of 0.588–0.948, except for spinel, with R^2 of 0.989). The mean free energy of sorption as estimated by the DR isotherm all give values be-

tween 8 and 16 kJ mol^{-1}, indicating that Ni sorption is mainly governed by ion exchange with the surfaces.

The sorption capacities comparison shown in Fig. 2 do not represent the total sorption capacities of the waste rock and pure mineral samples, but are a measure of their relative sorption capacities

Table 7
Results from XPS analyses in atomic percentage.

Sample	Al	C	Ca	Fe	Mg	N	Na	Ni	O	S	Si	Ti
Before Ni sorption												
Ilmenite TiO	2.6	26.3	0.6	5.9	3.2				52.1		6.2	2.7
Ilmenite NW	3.4	25.2	0.5	5.4	3.1				52.7		7.1	2.4
Plagioclase	6.6	21.1	0.8	1.4	1.4		0.8		53.9		13.7	0.3
Chlorite	4.5	23.2	0.5	3.5	3.3	0.7	0.2		54.7		9.0	0.6
Spinel	9.1	25.0	0.5	3.5	3.1	0.4	0.2		51.2		5.5	0.8
Mica	5.0	19.5		2.2	5.1		0.1		55.4		9.9	0.8
After Ni sorption												
Ilmenite TiO	0.8	15.6		4.8	0.4	8.9	8.8	3.2	53.5	0.4	2.1	1.1
Ilmenite NW	1.3	18.0		4.6	0.6	7.4	8.0	4.5	52.6	0.3	1.4	1.1
Plagioclase	3.2	12.0		0.4	0.2	7.7	8.3	5.6	56.9	0.3	5.3	0.1
Chlorite	2.9	11.2	0.3	3.4	2.0	4.7	4.0	6.4	58.6		5.9	0.1
Spinel	3.0	15.2		2.6	1.1	9.6	9.0	2.6	53.9	0.3	2.3	0.4
Mica	4.0	11.5	0.3	3.3	3.4	2.5	3.4	4.6	57.0		7.5	0.9
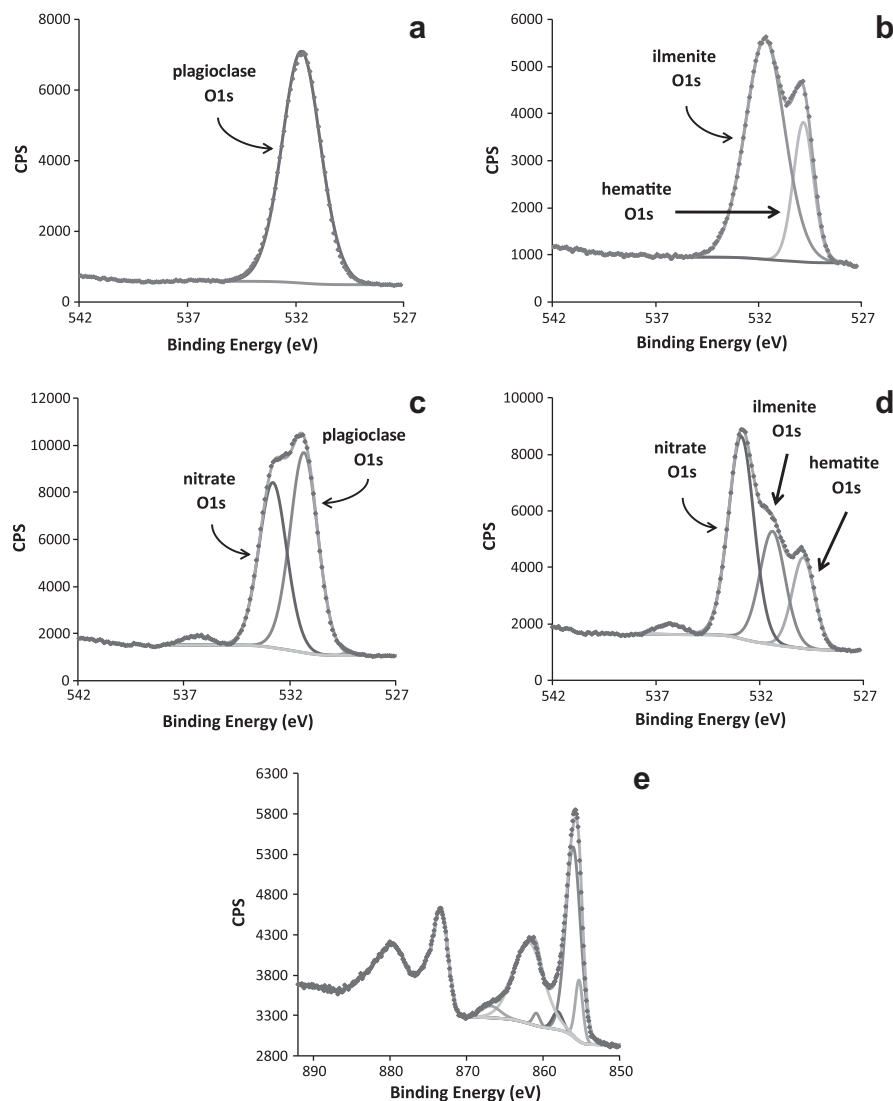
Fig. 4. XPS spectra of plagioclase O window before (a) and after (c) sorption, ilmenite O window before (b) and after (d) sorption, and plagioclase Ni(OH)$_2$ spectrum window (e) after sorption with 25 mg L^{-1} Ni at pH 6.

when in contact with aqueous Ni until equilibrium is reached. The sorption results demonstrate that the weathered waste rock Ni sorption capacities are less than for fresh ones. They also demonstrate that plagioclase is the most effective Ni-retaining material in the waste rocks on a surface basis, followed by hemo-ilmenite. Since those minerals represent the major mineralogy of the waste rocks (between 76 and 80 wt.% of the waste rock samples studied), sorption by other minor minerals seems to be less significant. To better characterize the sorption characteristics of the Tio waste rock, other characterization tests were performed after some sorption tests: sequential extractions, XPS analyses and DRIFT analyses. The main results are discussed in the following along with interpretations.

4.6. Sequential extractions

Sequential extractions were performed on waste rock samples C1–C6 in order to estimate the nature of the sorption sites; these results are presented in Table 9 and illustrated in Fig. 3a and b. Between 91% and 97% of the extracted Ni comes from reducible phases. The Ni extracted from the soluble and exchangeable fractions accounts for 2.5–4.6% of the extracted Ni in the fresh and for 3.6–7.2% in the weathered waste rock samples. The Ni extracted from the acid soluble fraction represents only 0.1–0.3% in the fresh and 1.1–1.5% in the weathered waste rock samples. These results suggest that even though the weathered waste rocks offer more acid-soluble and soluble/exchangeable sorption sites than the fresh ones, the main sorption sites consist of reducible species, and other sorption sites remain almost negligible. These reducible species are generally considered to be Fe and Mn oxides and oxy-hydroxides. However, no such species are identified on the waste rock and pure mineral samples with the characterization methods used in the present study. The reducible species may be the O atoms at the ilmenite, hematite and plagioclase surface. Since the O atoms are more electronegative than the other elements in the crystal lattice of the hematite, ilmenite and plagioclase, they bear a negative charge likely to be responsible for Ni sorption onto mineral surfaces.

4.7. XPS analysis

The chemical analyses performed with XPS survey scans on the pure mineral samples prior and after Ni sorption are given in Table 7. Nickel is below the XPS detection limit for all samples prior to Ni sorption, and is detected in all samples after Ni sorption, from 2.6 to 6.4 wt.%. Sodium and N contents are also considerably higher after Ni sorption on all samples analyzed, probably from the $NaNO_3$ matrix in which the sorption tests were conducted. Aluminium, C, Ca, Fe, Mg, Si and Ti were detected at lower concentrations for samples from Ni-sorption experiments than the initial materials. The
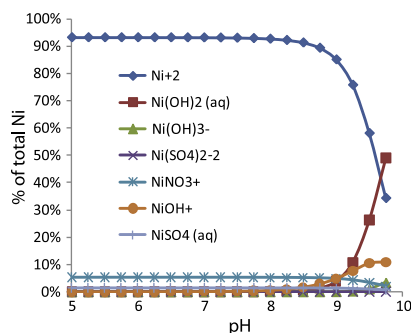
Ni contents on the samples after sorption as determined by XPS do not follow those of the sorption capacities shown in Fig. 2, because the XPS only considers the surface of the samples in the quantifications, while the sorption capacities are determined with the total sample mass. Therefore, Ni is more concentrated on the surface than over the entire bulk sample, which explains the difference in chemical compositions determined by XPS and by comparing the sorbed Ni over the whole sample mass, as is done in sorption experiments.

The high resolution XPS spectra of pure minerals before and after sorption showed significant differences for the Ni2p and O1s regions. Examples of XPS spectra are shown in Fig. 4 for plagioclase O1s before Ni sorption (a) and after Ni sorption (c), ilmenite O1s before (b) and after (d) sorption and Ni2p after sorption (e). Prior to sorption, the O1s region showed a single broad peak for silicates and spinel around 531.7 eV (Fig. 4a – plagioclase), and the ilmenite O1s region showed two peaks at 531.7 and 529.8 eV (Fig. 4b). After sorption, an extra O1s peak appears at 532.8–532.9 eV (Fig. 4c and d for plagioclase and ilmenite, respectively). No Ni was detected by XPS on the pure mineral samples prior to sorption tests, while Ni was detected on all samples after sorption with a combination of six peaks between 855.3 and 866.8 eV (Fig. 4e – plagioclase). The Ni2p peaks are all attributed to $Ni(OH)_2$ species and are almost identical to a $Ni(OH)_2$ reference (Biesinger et al., 2009). The presence of $Ni(OH)_2$ in the samples after sorption is consistent with the sequential extraction results (Section 4.6), that show most of the Ni is in reducible phases, such as oxides and hydroxides. No Ni was detected on the samples prior to sorption.

The O1s peaks in the ilmenite samples before sorption (Fig. 4b) are attributed to ilmenite and hematite. The 529.8 eV peak is attributed to hematite (Lü et al., 1999; Desai et al., 2005; Fujii et al., 2008) and the 531.7 eV peak is attributed to ilmenite. The ratio of 75% and 25%, respectively, attributed to ilmenite and hematite is consistent with the ilmenite/hematite ratio in the ore (Table 4). The single O1s peak in the other pure mineral samples show that O is associated mainly with one component and is consistent with the range of other O1s peaks in oxides and silicates (Nesbitt et al., 2004; Zakaznova-Herzog et al., 2006, 2008; Dalby et al., 2007). The appearance of a new O1s peak around 532.8 eV after sorption (Fig. 4c and d) is most likely due to NO_3 from the 0.05 M $NaNO_3$ solution matrix (Bandis et al., 1999). The appearance of $Ni(OH)_2$ upon Ni sorption was observed on Al-bearing clay minerals and oxides at pH levels for which aqueous $Ni(OH)_2$ is negligible (d'Espinose de la Caillerie et al., 1995; Scheidegger et al., 1998; Scheinost et al., 1999). However, it is unclear whether the $Ni(OH)_2$ and NO_3 peaks detected on the sorbed samples were sorbed on the surface or left over after water evaporation in the XPS vacuum chamber prior to analysis, or a combination of both.

Fig. 5. Ni species distribution for 25.0 mg L^{-1} Ni and 12.5 mg L^{-1} SO$_4^{2-}$ in 0.05 M NaNO$_3$ medium.
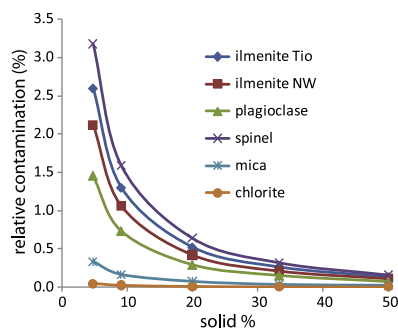
Fig. 6. Theoretical evaluation of the influence of the pulp solid content deposited in the XPS sample chamber on the relative Ni contamination of the surface quantifications.
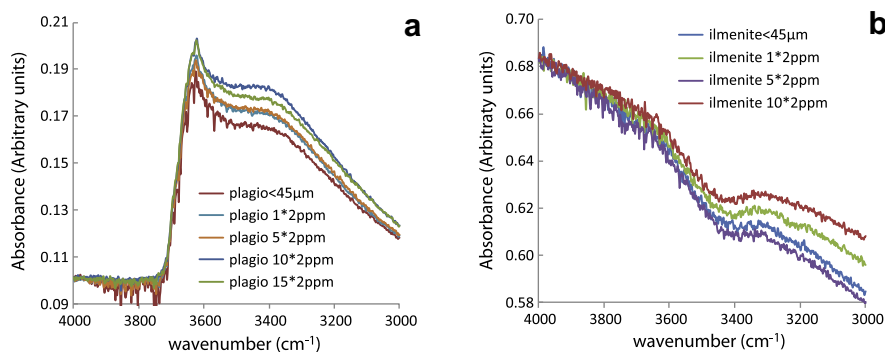
Fig. 7. Partial DRIFT spectra showing hydroxide region for successive sorption phases on plagioclase (a) and ilmenite (b).

Fig. 5 shows the results of thermodynamic simulations performed with Vminteq for the conditions of the sorption studies submitted to XPS analyses (25 mg L^{-1} Ni, 12.5 mg L^{-1} SO$_4$ in 0.05 M NaNO$_3$). In these conditions, aqueous Ni(OH)$_2$ only becomes significant over pH 8.5–9, under which the most significant aqueous Ni species is Ni^{2+}. Consequently, the Ni(OH)$_2$ phase is more likely a result of sorption rather than a phase already present in solution that is precipitated on the surface upon water evaporation.

An attempt was made to estimate the proportion of Ni detected by XPS on the surfaces that was attributable to residual aqueous Ni precipitated upon water evaporation in the sample chamber. The amount of precipitated Ni will depend on the aqueous Ni concentration and water volume within the aliquot put in the XPS sample chamber. Since the sample put in the XPS chamber was arbitrarily withdrawn from the bulk sample, it is impossible to know the sample's exact solid content. However, the residual Ni concentrations were noted in the course of the batch sorption tests that produced the samples submitted to XPS analyses. Estimations of the contamination were made on the basis of solid% of the sample put in the XPS chamber (see Fig. 6). The estimations shown in Fig. 6 suggest that water evaporation in the sample chamber cannot account for more than 3.2% of the detected Ni for a 5% solid pulp deposited in the sample chamber (for example, 50 mg sample in 0.95 mL or 950 mg water), which is probably less than the actual solid content of the pulp sample. Consequently, the Ni(OH)$_2$ detected on the surfaces upon Ni sorption by XPS are very likely the result of sorption processes rather than a result of residual aqueous Ni precipitation during sample preparation in the XPS chamber.

4.8. DRIFT analysis

The formation of a hydroxide phase on the surface with Ni sorption is also suggested by the DRIFT results (Fig. 7). DRIFT spectra were collected after submitting pure plagioclase and ilmenite samples to successive batch sorption tests (samples collected after 1, 5, 10 and 15 runs) at 2 mg L^{-1} Ni, pH 6. The OH stretching band at 3420 cm^{-1} (Caldeira et al., 2003) of the plagioclase sample

(Fig. 7a) shows a slight increase from 1 to 10 successive sorption tests, but the hydroxide peak after 15 runs is smaller than the peak obtained after 10 runs. The oxyhydroxides OH stretching band at 3630 cm^{-1} also increases slightly with successive sorption tests. The intensity of the OH stretching frequencies of the ilmenite samples (Fig. 7b) are difficult to interpret because of the absence of a baseline for proper comparison. A slight increase of the OH stretching bands at 3420 and 3630 cm^{-1} is noted for runs 1 and 10 in comparison to run 5 and the initial ilmenite sample. However, the differences in DRIFT spectra are subtle and the surface modifications associated with Ni batch sorption tests seem to be close to the detection limits of the DRIFT conditions employed in this study. No significant differences are observed over the rest of the plagioclase DRIFT spectra.

4.9. Possible sorption mechanisms

The formation of Ni(OH)$_2$ upon Ni sorption has also been observed in other studies (Eick and Fendorf, 1998; Scheidegger et al., 1997, 1998; Ford et al., 1999; Scheinost et al., 1999; Scheinost and Sparks, 2000; Scheckel et al., 2000; Elzinga and Sparks, 2001; Scheckel and Sparks, 2001a,b). The detection of the sorbed Ni(OH)$_2$ on the mineral surfaces may be explained by a sorption mechanism similar to the following (adapted from Bradbury and Baeyens (2009)):

$$\equiv S{-}OH + Ni^{2+} + 2H_2O \Longleftrightarrow \equiv S{-}O{-}Ni(OH)_2 + 2H^+ \qquad (13)$$
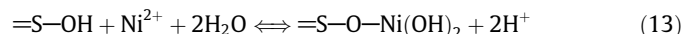
where $\equiv S{-}OH$ is a sorption site and $\equiv S{-}O{-}Ni(OH)_2$ is the surface site/Ni(OH)$_2$ complex. James and MacNaughton (1977) proposed a multistep mechanism for the sorption of the Ni^{2+} leading to the sorbed Ni(OH)$_2$:

$$\equiv S + Ni^{2+} \Longleftrightarrow \equiv S{-}Ni^{2+} \qquad (14)$$

$$\equiv S{-}Ni^{2+} + H_2O \Longleftrightarrow \equiv S{-}NiOH^+ + H^+ \qquad (15)$$

$$\equiv S{-}NiOH^+ + H_2O \Longleftrightarrow \equiv S{-}Ni(OH)_2 + H^+ \qquad (16)$$
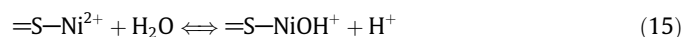
Echeverría et al. (2003) proposed different possibilities for Ni sorption onto e illite surface where hydrolyzed Ni species are involved, where $\equiv S{-}Na$ and $\equiv S{-}NiOH$ are surface species:

$$Ni^{2+} + 6H_2O \Longleftrightarrow Ni(OH)(H_2O)_5^+ + H^+ \qquad (17)$$

$$\equiv S{-}Na + Ni(OH)(H_2O)_5^+ \Longleftrightarrow \equiv S{-}NiOH + Na^+ \qquad (18)$$

$$\equiv S{-}Na + H_2O + Ni^{2+} \Longleftrightarrow \equiv S{-}NiOH + Na^+ + H^+ \qquad (19)$$
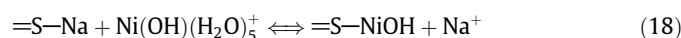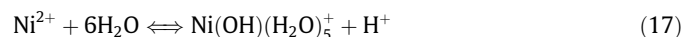
While the sorption mechanisms shown above are acid-producing, Sharma et al. (2009) proposed a sorption mechanism taking into account the hydrolyzed species which requires the presence

Table 8
Sequential chemical extraction steps.

Extraction step	Conditions	Liquid/solid ratio
Soluble/exchangeable	Magnesium chloride (MgCl$_2$) 0.5 M, pH 7, 1 h	24/1
Acid soluble	Sodium acetate (CH$_3$CH$_2$CO$_2$Na) 1 M, pH 5, 5 h	24/1
Reducible phases (Fe and Mn oxides and oxyhydroxides)	Hydroxylamine hydrochloride (NH$_2$OH{-}HCl) 0.04 M in 25% acetic acid (96 ± 3%), 6 h	36/1

Table 9
Sequential extraction results.

	Sorbed quantities (mg kg^{-1})			
	Soluble/exchang.	Acid soluble	Reducible phases	Total
C1				
Dup 1	2.47	0.141	50.1	52.7
Dup 2	2.42	0.145	50.2	52.8
Mean	2.45	0.143	50.1	52.7
Standard dev.	0.033	0.003	0.045	0.016
C2				
Dup 1	3.50	0.559	130	134
Dup 2	3.36	0.359	134	138
Mean	3.43	0.459	132	136
Standard dev.	0.092	0.142	2.99	2.75
C3				
Dup 1	3.03	0.121	117	121
Dup 2	3.05	0.121	116	119
Mean	3.04	0.121	117	120
Standard dev.	0.017	0.000	1.29	1.27
C4				
Dup 1	4.15	1.00	51.8	57.0
Dup 2	4.51	0.816	57.2	62.6
Mean	4.33	0.907	54.5	59.8
Standard dev.	0.258	0.129	3.82	3.95
C5				
Dup 1	1.69	0.458	44.8	47.0
Dup 2	1.68	0.567	43.3	45.5
Mean	1.69	0.513	44.0	46.2
Standard dev.	0.011	0.077	1.10	1.03
C6				
Dup 1	2.21	0.624	55.80	58.63
Dup 2	2.16	0.618	54.18	56.96
Mean	2.19	0.621	54.99	57.80
Standard dev.	0.032	0.004	1.15	1.18

of OH$^-$ in solution. Firstly, the hydrolyzed octahedral Ni^{2+} species ($Ni(H_2O)_6^{2+}$) may exchange two coordinated H$_2$O units for two OH$^-$ units (Eqs. (20) and (21)). Then, the Ni hydroxide precipitates or sorbs onto the surface while releasing four H$_2$O units (Eq. (22)). This mechanism is summarized in Eq. (23).

$$Ni(H_2O)_6^{2+} + OH^- \Longleftrightarrow Ni(OH)(H_2^O)_5^+ + H_2O \qquad (20)$$

$$Ni(OH)(H_2O)_5^+ + OH^- \Longleftrightarrow Ni(OH)_2(H_2O)_4 + H_2O \qquad (21)$$

$$Ni(OH)_2(H_2O)_4 \Longleftrightarrow Ni(OH)_2 \downarrow + 4H_2O \qquad (22)$$

$$Ni(H_2O)_6^{2+} + 2OH^- \Longleftrightarrow Ni(OH)_2 \downarrow + 6H_2O \qquad (23)$$
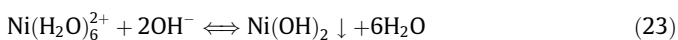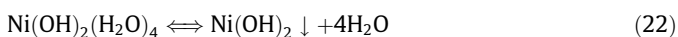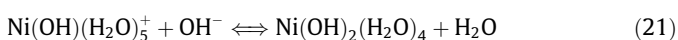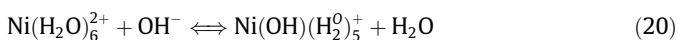
The surface species (≡S—OH) have been deliberately left out in the last mechanism (Eqs. (20)–(23)) because it is unclear whether the sorption sites are involved at the beginning of the process (ligand exchange, Eqs. (20) and (21)) or at the very end (formation of the hydroxide, Eq. (22)). Even though many different mechanisms are considered for the formation and sorption of the Ni(OH)$_2$, it is impossible to determine exactly which mechanisms are involved in Ni sorption on the waste rocks based on the results from the present study. Additional insight is needed in order to understand the precise sorption mechanisms involved.

It appears that the sorption phenomena in the fresh Tio waste rocks are mainly attributed to plagioclase and ilmenite minerals, due to their high sorption capacities normalized to surface area and to the fact that they represent more than 80 wt.% of the waste rock composition. However, the sorption properties of ageing ilmenite and plagioclase surfaces were not directly studied.

Consequently, the major sorption phases in weathered waste rock samples remain unclear.

Sorption seems to be associated with the formation of a hydroxide species similar to Ni(OH)$_2$ at the mineral surfaces, as supported by XPS data on pure mineral samples freshly sorbed with Ni. The formation of a hydroxide species is also suggested by the DRIFT spectral data collected on a Ni sorbed plagioclase sample, and also by the sequential extraction procedure, which showed that the majority of the Ni is extracted with the reducible fractions, believed to dissolve oxides and oxyhydroxides. The fact that the plagioclase DRIFT hydroxide peak slightly decreases after 15 runs with regards to 10 and 5 sorption runs may suggest the hypothesis that a hydroxide phase is building up on the plagioclase surface with Ni successive sorption tests up to 10 runs, but that by run 15 the conversion from Ni(OH)$_2$ to a Ni—Al LDH and/or Ni-phyllosilicate has started, thus diminishing the intensity of the associated hydroxide peaks. Such species were shown to develop with ageing upon Ni sorption on aluminosilicates; the Ni(OH)$_2$ species is believed to be formed during sorption, but with ageing, the surface precipitates would transform into Ni—Al layered double hydroxides (Ni—Al LDH), which in turn transformed into more stable Ni-phyllosilicates (Ford et al., 1999; Scheckel et al., 2000; Scheinost and Sparks, 2000; Scheckel and Sparks, 2001a,b). In the literature hereby stated on Ni—Al LDH and Ni phyllosilicates, these species were identified using a combination of diffuse reflectance spectroscopy, high-resolution thermogravimetric analysis and extended X-ray absorption spectroscopy (EXAFS). However, the formation of such species in the Tio mine waste rocks has yet to be verified.

An attempt was made to estimate the sorption capacities of the simple mineral combinations from the capacities of each pure mineral determined from batch tests. The calculation is based on the weighted average of the pure mineral sorption capacities, using Eq. (24).

$$q_{total} = \%_{ilm}q_{e,ilm} + \%_{plagio}q_{e,plagio} + \%_{chl}q_{e,chl} \qquad (24)$$

where q_{total}, $q_{e,i}$ are the total sorption capacity and the sorption capacity at equilibrium of species i in a batch test, and% is the i species percentage. The estimations were performed using the q_e values obtained in the three different Ni concentrations studied (1, 10 and 25 mg L^{-1}), while the sorption capacity of the mineral combinations were evaluated for 5 mg L^{-1}. Correction factors were applied on the weighted average capacities obtained with the pure mineral capacities to report the capacities to 5 mg L^{-1}: these correction factors were of 5 for 1 mg L^{-1}, 1/2 for 10 mg L^{-1} and 1/5 for 25 mg L^{-1}.

These estimations are biased by many factors. Firstly, the batch tests were performed at a liquid to solid ratio of 25 mL g^{-1}; thus in the mineral combinations, each mineral in the combinations is at a ratio greater than 25 mg L^{-1} (equal to 25 divided by the% composition of the mineral) when considered in the combination. Secondly, the competition between the mineral surfaces for Ni sorption was not studied and thus certain mineral surfaces may be favored more than others, a factor not taken into account in the predictions. In addition, this prediction technique is only valid for a similar range of S_s values to those of the pure minerals used, as the link between S_s values and sorption capacities is not linear. Finally, the batch sorption tests of the mineral combinations were performed at Ni concentrations that differ from those of the pure minerals.

The prediction results are given in Table 10. The predicted capacities are all below those obtained with the real combination of minerals. The closest prediction results are obtained with the 1 mg L^{-1} q_e values, while those obtained with 10 mg L^{-1} are even farther from those obtained with 25 mg L^{-1}. Competition effects between mineral surfaces for Ni sorption might explain the gap between the predicted and obtained sorption capacities. Previous

Table 10
Estimation of the sorption capacities of the pure minerals samples.

Combinations	q_e Estimated (mg g^{-1})			q_e Obtained (mg g^{-1})
	5 q_e at 1 mg L^{-1}	1/2 q_e at 10 mg L^{-1}	1/5 q_e at 25 mg L^{-1}	
cl-1	0.117	0.109	0.086	0.124
cl-2	0.111	0.105	0.085	0.128
cl-3	0.111	0.105	0.101	0.121
cl-4	0.111	0.106	0.098	0.124
cl-5	0.114	0.107	0.090	0.128

studies have reported difficulty in applying a component additivity approach to describe sorption in complex mineral assemblages (e.g. Davis et al., 1998). Nevertheless, the predicted sorption capacities are 70–95 % those obtained for the combinations, which is close enough for a rough estimate of the sorption capacities. The results show that prediction of the sorption capacities of simple mixtures is feasible for the limited set of conditions where predictions were attempted: similar S_s values, pH 6, in 0.05 M NaNO$_3$ matrix, at a liquid/solid ratio of 25 mL g^{-1}.

5. Conclusions

The main conclusions from this study are:

- The minerals composing the Tio mine waste rocks possess different sorption capacities, with the plagioclase and ilmenite minerals being the major sorbing phases of the fresh waste rocks.
- The impact of weathering on sorption properties was not directly measured for purified mineral fractions; consequently, the major sorbing phases in the weathered waste rocks are uncertain.
- Sequential extractions suggest that most sorption sites are associated with reducible fractions.
- XPS studies on sorbed surfaces suggest that Ni is sorbed as the hydroxide, Ni(OH)$_2$.
- The semi-quantitative prediction of sorption capacities of simple mineral assemblages is feasible from the sorption capacities of the individual components.

The results from the present study provide useful information on sorption phenomena involved in the Tio mine waste rocks and enable further interpretation of Ni geochemistry in CND However, additional studies are needed to better understand the mechanisms involved in Ni sorption in the Tio mine waste rocks. More precisely, it is impossible to determine exactly which mechanisms are involved in Ni sorption on the waste rocks based on the results from the present study. Further insight is needed in order to understand the precise sorption mechanisms involved. Moreover, competition effects between Ni and other metals present in actual drainage waters, as well as competition effects between surfaces for metal sorption, could be studied further for a better understanding of the processes involved in the actual waste rock piles.

Acknowledgements

References

Álvarez-Valero, A.M., Sáez, R., Pérez-López, R., Delgado, J., Nieto, J.M., 2009. Evaluation of heavy metal bio-availability from Almagrera pyrite-rich tailings dam (Iberian Pyrite Belt, SW Spain) based on a sequential extraction procedure. J. Geochem. Explor. 102, 87–94.

Bandis, C., Scudiero, L., Langford, S.C., Dickinson, J.T., 1999. Photoelectron emission studies of cleaved and excimer laser irradiated single-crystal surfaces of NaNO$_3$ and NaNO$_2$. Surf. Sci. 442, 413–419.

Bhattacharyya, K.G., Sen Gupta, S., 2008. Influence of acid activation on adsorption of Ni(II) and Cu(II) on kaolinite and montmorillonite: kinetic and thermodynamic study. Chem. Eng. J. 136, 1–13.

Biesinger, M.C., Payne, B.P., Lau, L.W.M., Gerson, A., Smart, R.S.C., 2009. X-ray photoelectron spectroscopic chemical state quantification of mixed nickel metal, oxide and hydroxide systems. Surf. Interface Anal. 41, 324–332.

Bradbury, M.H., Baeyens, B., 2009. Sorption modelling on illite. Part I: Titration measurements and the sorption of Ni, Co, Eu and Sn. Geochim. Cosmochim. Acta 73, 990–1003.

Brunauer, S., Emmett, P.H., Teller, E., 1938. Adsorption of gases in multimolecular layers. J. Am. Chem. Soc. 60, 309.

Bussière, B., 2007. Colloquium 2004: Hydrogeotechnical properties of hard rock tailings from metal mines and emerging geoenvironmental disposal approaches. Can. Geotech. J. 44, 1019–1052.

Bussière, B., Dagenais, A.-M., Villeneuve, M., Plante, B., 2005. Caractérisation environnementale d'un échantillon de stériles de la mine Tio. Technical report. Unité de recherche et de service en technologie minérale (URSTM), Rouyn-Noranda, Québec, Canada.

Caldeira, C.L., Ciminelli, V.S.T., Dias, A., Osseo-Asare, K., 2003. Pyrite oxidation in alkaline solutions: nature of the product layer. Int. J. Miner. Process. 72, 373–386.

Chen, Z., Xing, B., McGill, W.B., 1999. A unified sorption variable for environmental applications of the Freundlich equation. J. Environ. Qual. 28, 1422–1428.

Chen, Z., Ma, W., Han, M., 2008. Biosorption of nickel and copper onto treated alga (Undaria pinnatifida): application of isotherm and kinetic models. J. Hazard. Mater. 155, 327–333.

Coles, C.A., Yong, R.N., 2006. Use of equilibrium and initial metal concentrations in determining Freundlich isotherms for soils and sediments. Eng. Geol. 85, 19–25.

Dalby, K.N., Nesbitt, H.W., Zakaznova-Herzog, V.P., King, P.L., 2007. Resolution of bridging oxygen signals from O 1 s spectra of silicate glasses using XPS: Implications for O and Si speciation. Geochim. Cosmochim. Acta 71, 4297–4313.

Davis, J.A., Coston, J.A., Kent, D.B., Fuller, C.C., 1998. Application of the surface complexation concept to complex mineral assemblages. Environ. Sci. Technol. 32, 2820–2828.

Desai, J.D., Pathan, H.M., Min, S.-K., Jung, K.-D., Joo, O.S., 2005. FT-IR, XPS and PEC characterization of spray deposited hematite thin films. Appl. Surf. Sci. 252, 1870–1875.

D'Espinose De La Caillerie, J.B., Kermarec, M., Clause, O., 1995. Impregnation of γ-alumina with Ni(II) or Co(II) ions at neutral pH: Hydrotalcite-type coprecipitate formation and characterization. J. Am. Chem. Soc. 117, 11471–11481.

Echeverría, J., Indurain, J., Churio, E., Garrido, J., 2003. Simultaneous effect of pH, temperature, ionic strength, and initial concentration on the retention of Ni on illite. Colloids Surf. A: Physicochem. Eng. Aspects 218, 175–187.

Eick, M.J., Fendorf, S.E., 1998. Reaction sequence of Nickel(II) with kaolinite: mineral dissolution and surface complexation and precipitation. Soil Sci. Soc. Am. J. 62, 1257–1267.

Elzinga, E.J., Sparks, D.L., 2001. Reaction condition effects on nickel sorption mechanisms in illite-water suspensions. Soil Sci. Soc. Am. J. 65, 94–101.

Ford, R.G., Scheinost, A.C., Scheckel, K.G., Sparks, D.L., 1999. The link between clay mineral weathering and the stabilization of Ni surface precipitates. Environ. Sci. Technol. 33, 3140–3144.

Fujii, T., Takada, Y., Nakanishi, M., Takada, J., Kimura, M., Yoshikawa, H., 2008. Electronic structure of stoichiometric and non-stoichiometric epitaxial FeTiO$_3$ films. J. Phys. Conf. Ser. 100.

Grosvenor, A.P., Biesinger, M.C., Smart, R.S.C., McIntyre, N.S., 2006. New interpretations of XPS spectra of nickel metal and oxides. Surf. Sci. 600, 1771–1779.

Gu, X., Evans, L.J., 2007. Modelling the adsorption of Cd(II), Cu(II), Ni(II), Pb(II), and Zn(II) onto Fithian illite. J. Colloid Interface Sci. 307, 317–325.

Gunsinger, M.R., Ptacek, C.J., Blowes, D.W., Jambor, J.L., Moncur, M.C., 2006. Mechanisms controlling acid neutralization and metal mobility within a Ni-rich tailings impoundment. Appl. Geochem. 21, 1301–1321.

Hasan, S.H., Srivastava, P., Talat, M., 2009. Biosorption of Pb(II) from water using biomass of Aeromonas hydrophila: central composite design for optimization of process variables. J. Hazard. Mater. 168, 1155–1162.

Heikkinen, P.M., Räisänen, M.L., 2008. Mineralogical and geochemical alteration of Hitura sulphide mine tailings with emphasis on nickel mobility and retention. J. Geochem. Explor. 97, 1–20.

Heikkinen, P., Räisänen, M., Johnson, R., 2009. Geochemical characterisation of seepage and drainage water quality from two sulphide mine tailings impoundments: acid mine drainage versus neutral mine drainage. Mine Water Environ. 28, 30–49.

Ho, Y.S., Porter, J.F., McKay, G., 2002. Equilibrium isotherm studies for the sorption of divalent metal ions onto peat: copper, nickel and lead single component systems. Water Air Soil Pollut. 141, 1–33.

Holmström, H., Salmon, U.J., Carlsson, E., Petrov, P., Ohlander, B., 2001. Geochemical investigations of sulfide-bearing tailings at Kristineberg, Northern Sweden, a few years after remediation. Sci. Total Environ. 273, 111–133.

James, R.O., MacNaughton, M.G., 1977. The adsorption of aqueous heavy metals on inorganic minerals. Geochim. Cosmochim. Acta 41, 1549–1555.

Jeon, B.-H., Dempsey, B.A., Burgos, W.D., Royer, R.A., 2003. Sorption kinetics of Fe(II), Zn(II), Co(II), Ni(II), Cd(II), and Fe(II)/Me(II) onto hematite. Water Res. 37, 4135–4142.

Johnson, R.H., Blowes, D.W., Robertson, W.D., Jambor, J.L., 2000. The hydrogeochemistry of the Nickel Rim mine tailings impoundment, Sudbury, Ontario. J. Contam. Hydrol. 41, 49–80.

Landry, C.J., Koretsky, C.M., Lund, T.J., Schaller, M., Das, S., 2009. Surface complexation modeling of Co(II) adsorption on mixtures of hydrous ferric oxide, quartz and kaolinite. Geochim. Cosmochim. Acta 73, 3723–3737.

Li, M.G., 2000. Acid acid rock drainage prediction for low-sulfide, low-neutralization potential mine wastes. In: 5th International Conference on Acid Rock Drainage (ICARD). Denver, USA, pp. 567–580.

Limousin, G., Gaudet, J.P., Charlet, L., Szenknect, S., Barthes, V., Krimissa, M., 2007. Sorption isotherms: a review on physical bases, modeling and measurement. Appl. Geochem. 22, 249–275.

Lü, W., Yang, D., Sun, Y., Guo, Y., Xie, S., Li, H., 1999. Preparation and structural characterization of nanostructured iron oxide thin films. Appl. Surf. Sci. 147, 39–43.

McGregor, R.G., Blowes, D.W., Jambor, J.L., Robertson, W.D., 1998. Mobilization and attenuation of heavy metals within a nickel mine tailings impoundment near Sudbury, Ontario, Canada. Environ. Geol. 36, 305–319.

Nachtegaal, M., Sparks, D.L., 2003. Nickel sequestration in a kaolinite–humic acid complex. Environ. Sci. Technol. 37, 529–534.

Neculita, C.M., Zagury, G.J., Bussière, B., 2008. Effectiveness of sulfate-reducing passive bioreactors for treating highly contaminated acid mine drainage: II. Metal removal mechanisms and potential mobility. Appl. Geochem. 23, 3545–3560.

Nesbitt, H.W., Bancroft, G.M., Davidson, R., McIntyre, N.S., Pratt, A.R., 2004. Minimum XPS core-level line widths of insulators, including silicate minerals. Am. Mineral. 89, 878–882.

Nicholson, R.V., 2004. Overview of near neutral pH drainage and its mitigation: results of a MEND study. In: MEND Ontario Workshop, Sudbury, Canada, May 2004.

Özcan, A., Öncü, E.M., Özcan, A.S., 2006. Kinetics, isotherm and thermodynamic studies of adsorption of Acid Blue 193 from aqueous solutions onto natural sepiolite. Colloids Surf. A: Physicochem. Eng. Aspects 277, 90–97.

Pepin, G., 2009. Évaluation du comportement géochimique de stériles potentiellement générateurs de drainage neutre contaminé à l'aide de cellules expérimentales in situ. Master's thesis. École Polytechnique de Montréal, Montreal, Québec, Canada.

Pepin, G., Bussière, B., Aubertin, M., Benzaazoua, M., Plante, B., Laflamme, D., Zagury, G.J., 2008. Field experimental cells to evaluate the generation of contaminated neutral drainage by waste rocks at the Tio mine, Québec, Canada. In: Proceedings of 10th IMWA Congress on Mine Water and the Environment, Karlovy Vary, Czech Republic, pp. 309–312.

Pettit, C.M., Scharer, J.M., Chambers, D.B., Halbert, B.E., Kirkaldy, J.L., Bolduc, L., 1999. Neutral mine drainage. In: Proceedings of Sudbury 1999 Mining and the Environment International Conference, vol. 2, pp. 829–838.

Plante, B., 2010. Prediction du drainage neutre contaminé en Ni: cas de la mine Tio. Ph.D. thesis. Univ. Québec en Abitibi-Témiscamingue (UQAT), Québec, Canada.

Plante, B., Benzaazoua, M., Bussière, B., Pepin, G., Laflamme, D., 2008. Geochemical behavior of nickel contained in Tio mine waste rocks. In: Proceedings of 10th IMWA Congress on Mine Water and the Environment, Karlovy Vary, Czech Republic, pp. 317–320.

Pratt, A.R., Negeri, T., Deschênes, G., 2007. Analytical surface chemistry in mineral processing and hydrometallurgy. In: Proceedings of Canadian Mineral Processors 39th Annual Meeting, pp. 591–605.

Price, W.A., Kwong, Y.T.J., 1997. Waste rock weathering, sampling and analysis: observations from the British Columbia Ministry of Employment and Investment Database. In: Proceedings of 4th International Conference on Acid Rock Drainage (ICARD), Vancouver, pp. 31–45.

Rietveld, H.M., 1993. The Rietveld Method. Oxford University Press.

Scheckel, K.G., Sparks, D.L., 2001a. Temperature effects on nickel sorption kinetics at the mineral–water interface. Soil Sci. Soc. Am. J. 65, 719–728.

Scheckel, K.G., Sparks, D.L., 2001b. Division S-2 – soil chemistry: dissolution kinetics of nickel surface precipitates on clay mineral and oxide surfaces. Soil Sci. Soc. Am. J. 65, 685–694.

Scheckel, K.G., Scheinost, A.C., Ford, R.G., Sparks, D.L., 2000. Stability of layered Ni hydroxide surface precipitates – a dissolution kinetics study. Geochim. Cosmochim. Acta 64, 2727–2735.

Scheidegger, A.M., Lamble, G.M., Sparks, D.L., 1997. Spectroscopic evidence for the formation of mixed-cation hydroxide phases upon metal sorption on clays and aluminum oxides. J. Colloid Interface Sci. 186, 118–128.

Scheidegger, A.M., Strawn, D.G., Lamble, G.M., Sparks, D.L., 1998. The kinetics of mixed Ni–Al hydroxide formation on clay and aluminum oxide minerals: a time-resolved XAFS study. Geochim. Cosmochim. Acta 62, 2233–2245.

Scheinost, A.C., Sparks, D.L., 2000. Formation of layered single- and double-metal hydroxide precipitates at the mineral/water interface: a multiple-scattering XAFS analysis. J. Colloid Interface Sci. 223, 167–178.

Scheinost, A.C., Ford, R.G., Sparks, D.L., 1999. The role of Al in the formation of secondary Ni precipitates on pyrophyllite, gibbsite, talc, and amorphous silica: a DRS study. Geochim. Cosmochim. Acta 63, 3193–3203.

Sen Gupta, S., Bhattacharyya, K.G., 2006. Adsorption of Ni(II) on clays. J. Colloid Interface Sci. 295, 21–32.

Sen Gupta, S., Bhattacharyya, K.G., 2008. Immobilization of Pb(II), Cd(II) and Ni(II) ions on kaolinite and montmorillonite surfaces from aqueous medium. J. Environ. Manage. 87, 46–58.

Sharma, P., Singh, G., Tomar, R., 2009. Synthesis and characterization of an analogue of heulandite: Sorption applications for thorium(IV), europium(III), samarium(II) and iron(III) recovery from aqueous waste. J. Colloid Interface Sci. 332, 298–308.

Subramanyam, B., Das, A., 2009. Study of the adsorption of phenol by two soils based on kinetic and isotherm modeling analyses. Desalination 249, 914–921.

Tan, X., Chen, C., Yu, S., Wang, X., 2008. Sorption of Ni²⁺ on Na-rectorite studied by batch and spectroscopy methods. Appl. Geochem. 23, 2767–2777.

Wang, X.-S., Huang, J., Hu, H.-Q., Wang, J., Qin, Y., 2007. Determination of kinetic and equilibrium parameters of the batch adsorption of Ni(II) from aqueous solutions by Na-mordenite. J. Hazard. Mater. 142, 468–476.

Zagury, G., Bedeaux, C., Welfringer, B., 2009. Influence of mercury speciation and fractionation on bioaccessibility in soils. Arch. Environ. Contam. Toxicol. 56, 371–379.

Zakaznova-Herzog, V.P., Nesbitt, H.W., Bancroft, G.M., Tse, J.S., 2006. High resolution core and valence band XPS spectra of non-conductor pyroxenes. Surf. Sci. 600, 3175–3186.

Zakaznova-Herzog, V.P., Nesbitt, H.W., Bancroft, G.M., Tse, J.S., 2008. Characterization of leached layers on olivine and pyroxenes using high-resolution XPS and density functional calculations. Geochim. Cosmochim. Acta 72, 69–86.